

Article

Characteristics and Estimation of Dew in the Loess Hilly Region of Northern Shaanxi Province, China

Zhifeng Jia ^{1,2,3,*} , Yingjie Chang ^{1,2,3}, Hao Liu ^{1,2,3}, Ge Li ^{1,2,3}, Zilong Guan ⁴ , Xingchen Zhang ⁴, Ruru Xi ^{1,2,3}, Pengcheng Liu ^{1,5} and Yu Liu ⁶

¹ School of Water and Environment, Chang'an University, Xi'an 710054, China; 2021129001@chd.edu.cn (Y.C.); 2023129009@chd.edu.cn (H.L.); 2022229047@chd.edu.cn (G.L.); 2022129014@chd.edu.cn (R.X.); liupengcheng9611@163.com (P.L.)

² Key Laboratory of Subsurface Hydrology and Ecological Effects in Arid Region, Ministry of Education, Chang'an University, Xi'an 710054, China

³ Key Laboratory of Eco-Hydrology and Water Security in Arid and Semi-Arid Regions of the Ministry of Water Resources, Chang'an University, Xi'an 710054, China

⁴ PowerChina Northwest Engineering Corporation Limited, Xi'an 710065, China; hydgeo_guan@163.com (Z.G.); zhangxingchen66@126.com (X.Z.)

⁵ Xi'an Water (Group) Lijiahe Reservoir Management Company, Xi'an 710055, China

⁶ College of Water Resources and Architectural Engineering, Northwest A&F University, Yangling 712100, China; liuyu.chn@nwfau.edu.cn

* Correspondence: 409538088@chd.edu.cn; Tel.: +86-15829012186

Abstract: As a non-precipitation water source, dew is important for plant and animal survival and crop production in arid and water-scarce areas. This study assessed the amount of dew in a dry zone in a long-term (2016 to 2022) field observation experiment at the Ansai Experimental Station, a typical loess hilly area in China. Dew primarily occurred in summer and autumn, with a frequency of >50%. The average annual dew amount was 29.20 mm, with an average annual rainfall of 641.8 mm. The average annual dew-to-rain ratio was 4.58%, and the average annual number of dew days was 143.6 d/a. The surface soil moisture content increased by approximately 1.02% with increasing dew amounts. The change in the soil moisture at a 5 cm depth was 0.14% on average and lagged substantially by 1 h. Using the Beysens model, the annual estimated and measured dew amounts in 2022 were 25.27 and 29.84 mm, respectively, and the annual normalized root mean square deviation (NRMSD) was 0.17. Thus, the Beysens model evaluated the dew amount in the study area well at the monthly and annual scales. The quantification of dew resources can provide support for the development, utilization, and management of limited water resources in arid areas, promoting more accurate decision-making for the sustainable development of water resources in the future.

Keywords: dew; Beysens model; model estimation; loess hilly region; water ecosystem



check for updates

Citation: Jia, Z.; Chang, Y.; Liu, H.; Li, G.; Guan, Z.; Zhang, X.; Xi, R.; Liu, P.; Liu, Y. Characteristics and Estimation of Dew in the Loess Hilly Region of Northern Shaanxi Province, China. *Sustainability* **2024**, *16*, 2482. <https://doi.org/10.3390/su16062482>

Academic Editors: Wen-Ping Tsai, Yen-Ming Chiang and Yu-Jia Chiu

Received: 20 February 2024

Revised: 9 March 2024

Accepted: 10 March 2024

Published: 17 March 2024



Copyright: © 2024 by the authors. Licensee MDPI, Basel, Switzerland. This article is an open access article distributed under the terms and conditions of the Creative Commons Attribution (CC BY) license (<https://creativecommons.org/licenses/by/4.0/>).

1. Introduction

The arid and semi-arid regions of China cover an area of over 2.56 million km², constituting 26.7% of the country's total land area, and exhibiting water scarcity, vegetation cover degradation, and severe desertification [1,2]. As a typical arid and semi-arid region, the Loess Plateau is influenced by its special geological background and meteorological factors, with severe soil erosion, drought and water shortage, and a fragile ecological environment [3,4]. In this case, water shortages are an important factor limiting the growth and development of plants and crops [5–7]. Meanwhile, in arid and semi-arid zones, dew is an important source of water to sustain animals and plants [8,9] and alleviates water deficits in the soil–plant–atmosphere water cycle system continuum [10]. In extreme drought areas, dew may be the dominant factor for plant survival, with rainfall as a secondary factor [11]. Therefore, the observation and evaluation of dew resources are vital for the utilization and sustainable development of water resources in arid regions.

Dew refers to the condensation products that form when water vapor near the surface radiates heat away from plants or topsoil [12] when night-time temperatures approach or fall below the dew point [13]. At present, dew observation methods can be divided into two categories—direct observations and model evaluations. Direct observation methods include the lysimeter, leaf wetness sensor, Duvdevani dew meter, and Hiltner dew balance methods. However, the Duvdevani dew gauge and Hiltner dew balance methods impact the assessment of dew because the materials on a condenser surface differ from those of a natural plant system [14]. Thus, the lysimeter method is currently the ideal measurement method, primarily applied to soil condensation water [15]. However, although the observation accuracy of large-scale lysimeters is relatively high, the equipment cost is also high [16]. The leaf wetness sensor (LWS) uses bionic technology to mimic a real leaf and monitors water or ice on its surface via a highly sensitive dielectric constant with high accuracy, precisely measuring the duration of the persistence of dew on the surface of the leaf [17]. Therefore, LWS is widely used for dew field observations [18–21]. Field observations are generally single- or multiple-site observations with certain spatial scale limitations and require an extremely high instrumental accuracy. Therefore, there has been an increase in studies on the numerical or empirical modeling of condensate estimations. The Penman–Monteith formula considers both aerodynamics and crop physiological characteristics and is applied to farmland ecosystems [22]. However, the model assumes that the condensation environment is ideal, and it is difficult to satisfy the model requirements under natural conditions. The water vapor turbulence transport method, that is, the vorticity correlation method, tends to underestimate night-time low-turbulence conditions, resulting in low condensation amounts [23]. The surface energy balance method is suitable for condensate assessments on a large spatial scale [24]. In addition to long-term field observations, this study plans to use some easily available meteorological data to simulate the dew amount. Some scholars have conducted relevant studies [25,26]. For example, in the arid zone in southeastern Morocco, a neural network model was constructed to simulate the amount of urban dew using meteorological data on the atmospheric temperature, relative humidity, wind speed, and cloudiness at the test sites. The results showed that the amount of urban dew could be simulated using meteorological data [25]. The Beysens model was constructed using meteorological elements to simulate dew quantity and validated in 10 different regions worldwide [26]. However, the applicability of the Beysens model to arid regions in China needs further study.

To date, there has been a range of studies conducted on dew collection methods [27–29], formation conditions [13,30], measuring methods [8,31,32], influencing factors [33,34], characteristics of condensation [35,36], occurrence frequency [10,37], and ecohydrological effects [38,39]. However, there are differences in dew formation in different arid regions, and, to date, relatively few long-term dew observation studies have been conducted. In this study, a typical loess hilly area in China was selected to conduct long-term field observation experiments on dew from 2016 to 2022. The aims of this study were the following: (1) to observe the characteristics of dew formation, interannual variations, and influencing factors in the loess hilly region; (2) to estimate the amount of dew based on meteorological data using the Beysens model and to evaluate the applicability of the model by comparing it with the measured data; and (3) to explore the significance of dew for plant and animal survival and crop production. The results of this study can provide a basis for the sustainable development and utilization of dew resources and the protection of ecosystems in arid regions.

2. Materials and Methods

2.1. Study Area

The geographical location of the study area is shown in Figure 1. The experimental station (36°51'22" N, 109°18'58" E) is located at the Ansai Experimental Station of the Institute of Soil and Water Conservation, Chinese Academy of Sciences in Yan'an City, Shaanxi Province, China (Figure 1). The study area, at an elevation of 1068–1309 m is a

typical loess hilly and gully area with a mid-temperate continental semi-arid monsoon climate. The annual average temperature is 8.8 °C, the maximum temperature is 36.8 °C, and the minimum temperature is −23.6 °C. It is dry and cold in winter and spring, dry in summer, and cool and frosty in autumn. The average precipitation is 500 mm [40]. In addition, the frost-free period is approximately 157 d, the annual potential evaporation is 1010–1400 mm [41], and the sunshine hours are 2396 h·a^{−1} [42]. The vegetation types are primarily herbaceous communities and thickets, and the common plants include *Robinia*, *Pinus tabulaeformis*, *Caragana korshinskii*, and sea buckthorn [7,43].

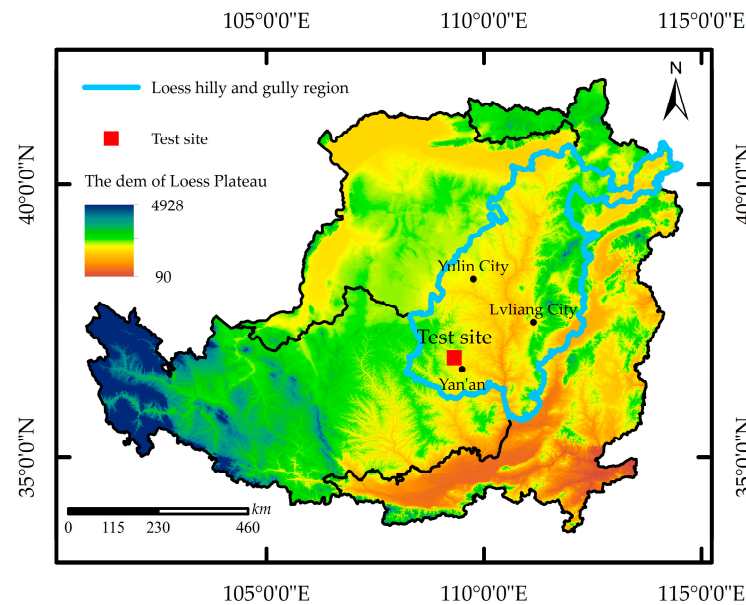


Figure 1. Geographic location of the experimental site.

2.2. Experimental Design

The instrument and site layouts for the dew field observations are shown in Figure 2. The experimental observation period was from 1 January 2016 to 31 December 2022. The dew amount was obtained based on the relationship between the micro-voltage (U) output of the LWS and the thickness of the water layer (see Section 2.3.1), and the dew persistence time (DT) was directly measured using the LWS. A VP-3 was used to measure the air temperature (T_{a20}) and relative humidity (RH), and the RH was measured by a capacitance-type sensor [44]. The wind speed (v_s) and wind direction (v_d) were monitored using a WSD01 anemometer. An ECRN-100 rain gauge was selected for the precipitation measurements. Two soil moisture sensors (Model GS3) were installed at 0 cm and 5 cm depths to monitor the soil temperature and soil water content (SWC_0 , SWC_5). All monitoring data were recorded at 30 min intervals using an EM50 collector. All the instruments were manufactured by Decagon Devices (Pullman, WA, USA). The accuracies and installation heights of the observation equipment are listed in Table 1.

Table 1. Accuracy and placement of instruments.

Instrument	Installation Height	Monitoring Index and Unit	Measurement Accuracy
Wind gauge	200 cm	$v_s, m \cdot s^{-1}; v_d, ^\circ$	$v_s: \pm 0.45 m \cdot s^{-1}; v_d: \pm 1^\circ$
ECRN-100	160 cm	Precipitation, mm	± 0.2 mm
LWS	20 cm	$U, mV; DT, min$	$U, \pm 1 mV; DT, \pm 1 min$
VP-3	20 cm	$T_{a20}, ^\circ C; RH, \%$	Temperature, $\pm 0.2 ^\circ C; RH, \pm 0.1\%$
GS3	0 cm, −5 cm	$T_{s0}, T_{s5}, ^\circ C;$ $SWC_0, SWC_5, m^3/m^3$	Temperature, $\pm 0.3 ^\circ C;$ $SWC, \pm 0.02 m^3/m^3$
EM50	120 cm	/	/

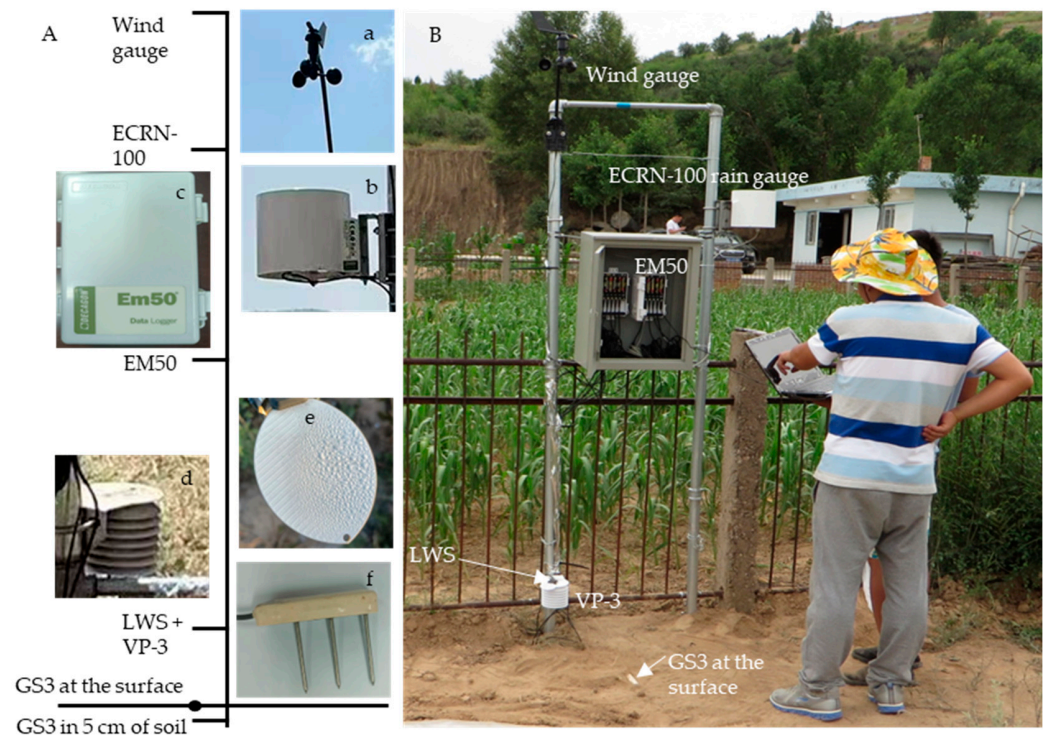


Figure 2. Equipment (A) and installation position (B): (a) wind gauge, (b) ECRN-100, (c) EM50, (d) VP-3, (e) LWS, and (f) GS3.

2.3. Data Processing

2.3.1. Dew Amount

A LWS was used to monitor the surface dew or frost. The relationship between the micro-voltage of the LWS and the thickness of the water layer (D_i) on the sensor surface was established by Jia et al. [17], as shown in Equation (1),

$$D_i = aU_i^b \quad (1)$$

where D_i is the dew on the surface of the LWS, with an accuracy of 0.02 mm; U_i is the output voltage of the sensor, mV; a and b are the fitting parameters; and $a = 4 \times 10^{-14}$, $b = 4.4188$ ($r = 0.9937$, $p < 0.01$).

The dew observation period was from 17:00 to 10:00 the following day. As dew occurred only during certain periods, the daily dew amount was defined as the sum of period condensation, as shown in Equation (2) [17]. This is similar to the data processing methods of other scholars [45,46].

$$D_d = \begin{cases} \sum_{i=1}^n (D_{it} - D_{i0}) & D_{it} \geq D_{i0} \\ 0 & D_{it} < D_{i0} \end{cases} \quad (2)$$

where D_d is the daily dew amount in mm, and n is the total number of daily intervals. In this study, the interval between observation periods was 30 min, then $n = 34$, $i = 1, 2, \dots, 34$. D_{i0} and D_{it} are the dew amounts at the initial and final moments of the observation period of i , respectively, in mm. When $D_{it} - D_{i0} \geq 0$, the period is the condensation stage; when $D_{it} - D_{i0} < 0$, the period is the evaporation stage. Specifically, in the dew calculation process, we excluded the observation data for periods in which rainfall occurred, to avoid the influence of rainfall on the dew observation [17].

2.3.2. Dew Point

The dew point was calculated using Equation (3) [47].

$$T_d = \frac{B_1 \left[\ln \left(\frac{H_R}{100} \right) + \frac{A_1 T_a}{B_1 + T_a} \right]}{A_1 - \left[\ln \left(\frac{H_R}{100} \right) + \frac{A_1 T_a}{B_1 + T_a} \right]} \quad (3)$$

where T_a and T_d are the air temperature and dew point temperature, respectively, °C; H_R is the RH of air, %; and A_1 and B_1 are the coefficients recommended by Alduchov and Eskridge, respectively. $A_1 = 17.625$, $B_1 = 243.04$ °C [48]. The air temperature (T_{a20}) and RH at 20 cm above the ground were used in this study.

2.3.3. Cloud Data

Cloud cover data were obtained from the Copernicus Climate Data Store [49] and expressed as a percentage of the sky area covered by clouds. For the dew simulations, the acquired cloud cover data were converted into an octant representation of the classical measurements using the Okta method [50]. Okta's method divides the sky into eight equal parts. If the sky is covered by N parts, the cloud amount is N ($N = 0, 1, 2, 8$) [51].

2.3.4. Relevant Definitions

(1) Average daily dew quantity:

$$\bar{D}_{di} = \frac{D_{mi}}{P0_i} \quad (4)$$

where \bar{D}_{di} is the average daily dew in the month i ($i = 1, 2, \dots, 12$), D_{mi} is the total monthly dew amount in the month i , and $P0_i$ is the number of days in the month i without rainfall.

(2) The dew occurrence frequency is defined as the ratio of the number of dew days ($D_d > 0$) in a certain observation period to the total number of days in the same period.

(3) The DT indicates the duration of dew persistence on the LWS surface. This is defined as the sum of the durations of the condensation and evaporation phases. The condensation duration was defined as the sum of all observation periods in which the dew amount at the end of a single observation period (D_{it}) was greater than or equal to that at the beginning of the single observation period (D_{i0}). The evaporation duration was defined as the sum of all observation periods in which the amount of dew at the end of a single observation period (D_{it}) was less than that at the initial moment of the observation period (D_{i0}), and the interval between observation periods was 30 min.

(4) The dew-to-rain ratio is defined as the ratio of dew amount to the precipitation over a certain observation period.

2.4. Dew Estimation

2.4.1. Beysens Model

The amount of dew was estimated using the Beysens model with the following equation [26]:

$$\frac{dh}{dt} = \begin{cases} m \frac{(1 - \varepsilon_s)}{0.2422} \times \left(\frac{T_d + 273.15}{285} \right)^4 \left(1 - \frac{N}{8} \right) + \alpha (T_d - T_a) \times C \left(\frac{v_s}{v_0} \right) & v_s < v_0 \\ 0 & v_s > v_0 \end{cases} \quad (5)$$

where m and α are parameters, $m = 0.37$ mm·d⁻¹, $\alpha = 0.06$ mm·d⁻¹·K⁻¹; ε_s is the atmospheric emissivity; N is the cloudiness data expressed in terms of Okta classical measurements; T_d is the dew point temperature, °C; T_a is the air temperature, °C; and v_s and v_0 are the momentary wind speed and critical wind speed, respectively, m·s⁻¹. Equation (5) has been tested and validated in 10 different climate sites in the world, and m and α exhibited good applicability [26].

The coupling of wind and natural convection enhances the convective heat transfer, and the effect of wind speed on dew can be determined using Equation (6) [26]. During the observation process, there is an inevitable local airflow difference around the condensation surface, which affects the heat exchange between the condenser and the air [52]. In terms of the wind speed statistics at 200 cm above the ground, the dew frequency and the dew amount were extremely small when the wind speed was greater than $1.1 \text{ m}\cdot\text{s}^{-1}$. Therefore, the critical wind speed (v_0) was determined as $1.1 \text{ m}\cdot\text{s}^{-1}$.

$$C(v_s/v_0) = 1 + 100 \times \left\{ 1 - \exp \left[- \left(\frac{v_s}{v_0} \right)^{20} \right] \right\} = \begin{cases} 1, & v_s < v_0 \\ 101, & v_s > v_0 \end{cases} \quad (6)$$

Atmospheric emissivity is a function of the water vapor content of air. It can be estimated from the elevation H of the dew point observation site using the following formula [53].

$$1 - \varepsilon_s = 0.2422 \times \left[1 + 0.204323H - 0.0238893H^2 - \left(18.0132 - 1.04963H + 0.21891H^2 \right) \times 10^{-3}T_d \right] \quad (7)$$

where T_d is the dew point temperature, °C, and H is the elevation of the experimental site in this study, 1.1 km.

2.4.2. Error Evaluation

The normalized root-mean-square deviation (NRMSD) is a metric used to measure the accuracy of predictive models [54,55]. The NRMSD at the monthly and annual scales was used to determine how well the simulated values of dew matched the measured values using Equation (8) [56].

$$\text{NRMSD} = \frac{\sqrt{\sum_{i=1}^K \frac{(D_{di} - E_{di})^2}{K}}}{\max(D_{d1}, D_{d2}, \dots, D_{dK}) - \min(D_{d1}, D_{d2}, \dots, D_{dK})} \quad (8)$$

where D_{di} is the measured value of dew, mm, and E_{di} is the simulated value of dew, mm. $\max(D_{d1}, D_{d2}, \dots, D_{dK})$ and $\min(D_{d1}, D_{d2}, \dots, D_{dK})$ are the maximum and minimum values of dew measured during the observation period, respectively, and K is the total number of simulation days. Referring to the evaluation criteria of other studies, when $\text{NRMSD} < 0.52$, the model simulation results are acceptable [57,58].

2.5. Data Analysis

The Pearson correlation method [59,60] was used to analyze the simulation effect, which indicates a fitting degree between the simulated and measured dew values or the accuracy of the model simulation. OriginPro 2023 (OriginLab Corporation, Northampton, MA, USA) was used for data analysis and mapping.

3. Results

3.1. Dew Characteristics

3.1.1. Daily Variation of Dew

We selected 14 March 2021 (spring), 30 July 2022 (summer), 14 September 2021 (autumn), and 13 December 2021 (winter) as typical days to analyze the daily variation process of dew in different seasons, as shown in Figure 3. The dew process is similar among different seasons and can be divided into the condensation and evaporation stages (Figure 3a). The duration of the condensation stage was significantly longer than that of the evaporation stage. The proportion of the condensation duration was greater than 75% during the entire period (Figure 3b). As shown in Figure 3c–f, the meteorological and water vapor conditions with increasing RH and decreasing air temperature resulted in a decrease in the temperature dew point difference. This was conducive to the occurrence of dew in the condensation stage, and the dew peak appeared at 5:00–8:00 am. Although the RH was high during

the evaporation phase, the increased air temperature caused the temperature dew point difference to increase, which was not favorable for dew. The dew amount, condensation duration, and DT varied seasonally in the order of autumn > summer > spring > winter. The initial occurrence of dew in autumn was 2.5 h earlier than that in summer, 3.5 h earlier than that in spring, and 6 h earlier than that in winter (Figure 3a). This is related to changes in the RH and air temperature. In autumn, the RH was greater than 80% at 21:30, and the temperature dew point difference was less than 4 °C (Figure 3e), which more likely leads to dew occurrence. Meanwhile, in the evaporation stage after the dew peak, the air temperature approached the dew point. Therefore, the evaporation of dew was slower, and its persistence on the condensation surface was the longest in autumn at 12 h.

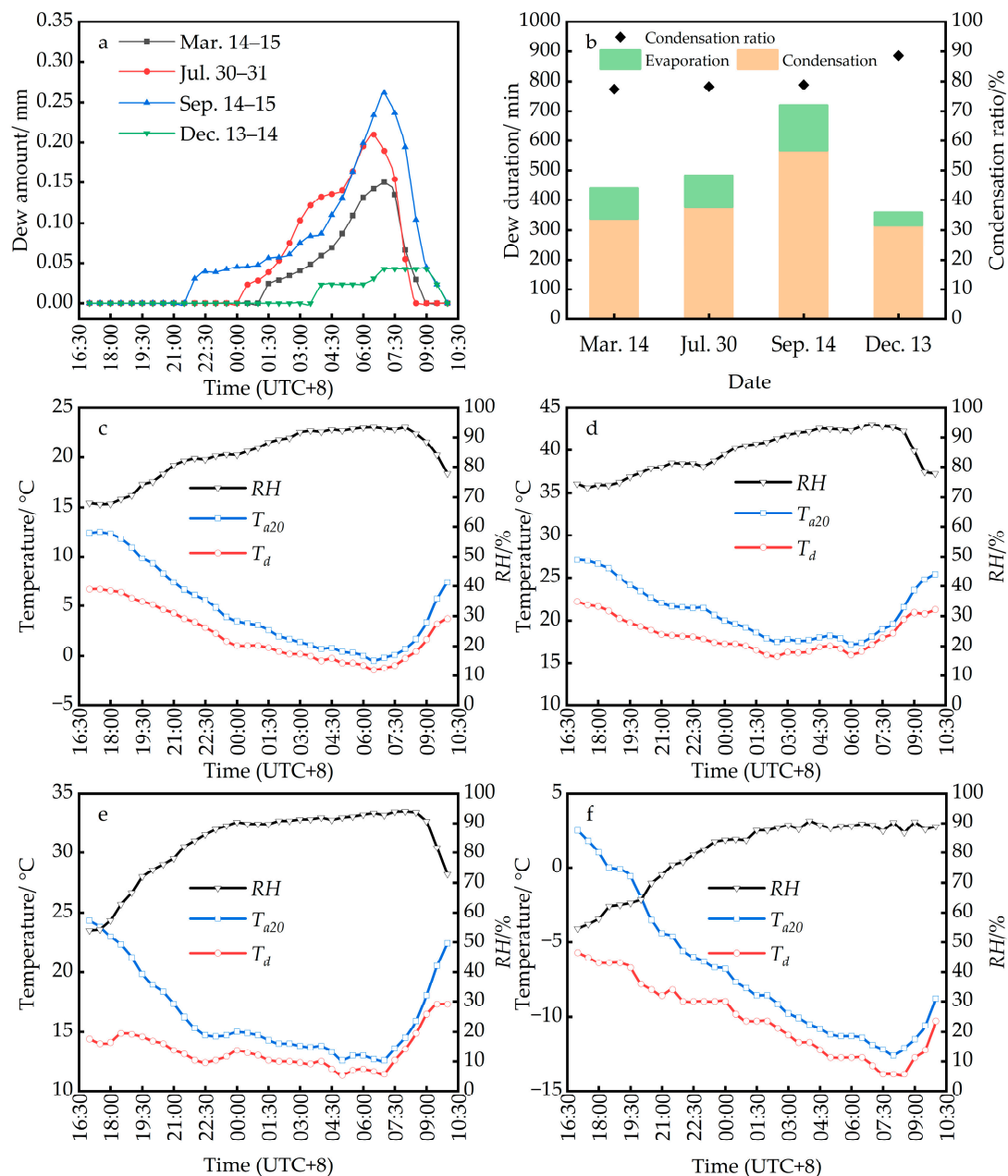


Figure 3. Daily variation of dew: (a) the process of dew on four typical days and (b) condensation duration, evaporation duration, and the percentage of condensation duration of dew in different seasons. (c–f) Daily variation of meteorological conditions on 14 March 2021, 30 July 2022, 14 September 2021, and 13 December 2021 (T_{a20} , air temperature at 20 cm; T_d , dew point at 20 cm; RH , relative humidity at 20 cm).

3.1.2. Monthly Dew Variation

The varying trend of dew in different months from 2016 to 2022 was analyzed and presented in Figure 4. The total monthly dew quantity, mean daily dew amount, monthly dew days, and monthly dew frequency exhibited an overall trend of increasing and then decreasing, with a peak in September. From the variations in the dew amount over the last seven years, the minimum value of the average daily dew amount was 0.16 mm in September, with more than 20 monthly dew days, and a monthly dew frequency greater than 65% (Figure 4b–d). Although the amount of dew varied annually, it was concentrated in summer (June–August) and autumn (September–November), with smaller amounts in winter (December–February) and spring (March–May). The months with an average monthly dew frequency greater than 50% were July–October, peaking in September (Figure 4d). The mean values of the total monthly dew quantity in July–October were 5.04, 4.93, 6.83, and 4.48 mm, respectively. The dew amount during this period accounted for approximately 72.9% of that of the entire year (Figure 4a).

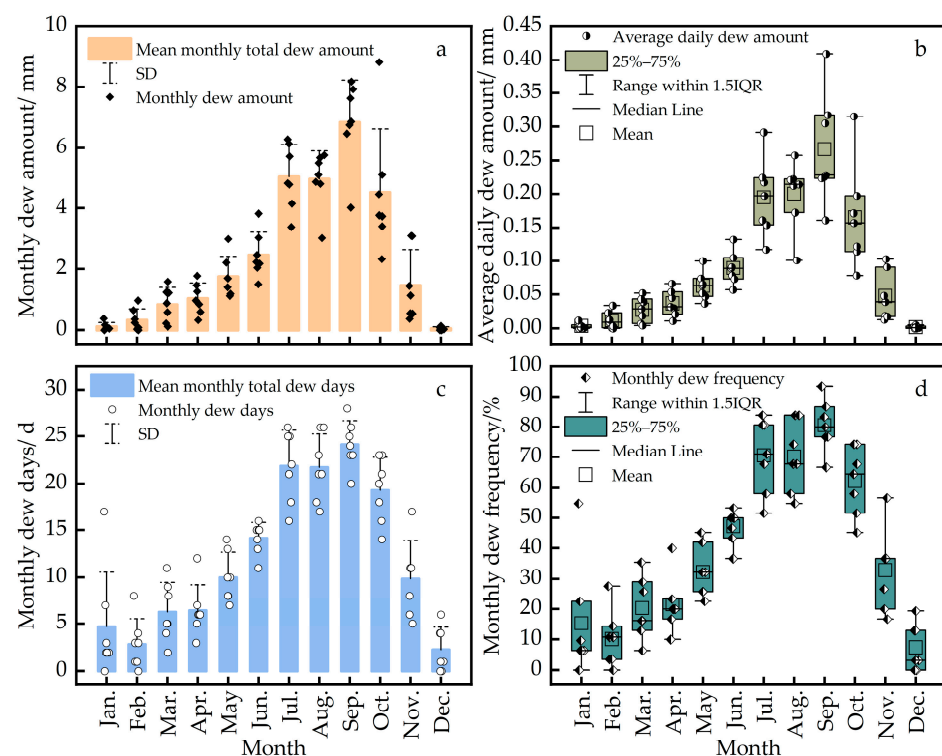


Figure 4. Monthly variation of dew amount: (a) total monthly dew amount (SD, standard deviation); (b) average daily dew amount; (c) monthly dew days; and (d) frequency of dew.

3.1.3. Annual Dew Variation

The interannual variation in dew and rainfall in different years is shown in Figure 5a. The dew-to-rain ratio showed a decreasing trend, then it increased and then decreased. The average annual dew ratio was 4.58%, the maximum dew ratio was 6.03% (2019), and the minimum was 4.02% (2022). When the rainfall was less than 650 mm, the amount of dew increased with the increase in rainfall, peaking in 2019. However, the dew amount began to decrease when the rainfall was greater than 650 mm (Figure 5b). Comparing the relationship between annual rainfall and total annual dew showed that a moderate amount of annual rainfall (<650 mm) is conducive to the amount of dew in loess hilly areas. The results of a study in Onne (Port Hartcourt), Nigeria, showed that dewfall was the highest in the months with moderate rainfall, and dew in months with high rainfall was smaller but higher than in months without rainfall [61]. This is consistent with the experimental results of this study. A moderate amount of rainfall could increase the water vapor content in the air, and the dew amount following rainfall was significantly and positively correlated with

rainfall [61,62]. Therefore, this study indicates that too little rainfall leads to insufficient water vapor, and too much rainfall leads to a decrease in the period of dewfall, neither of which are conducive to the occurrence of dew.

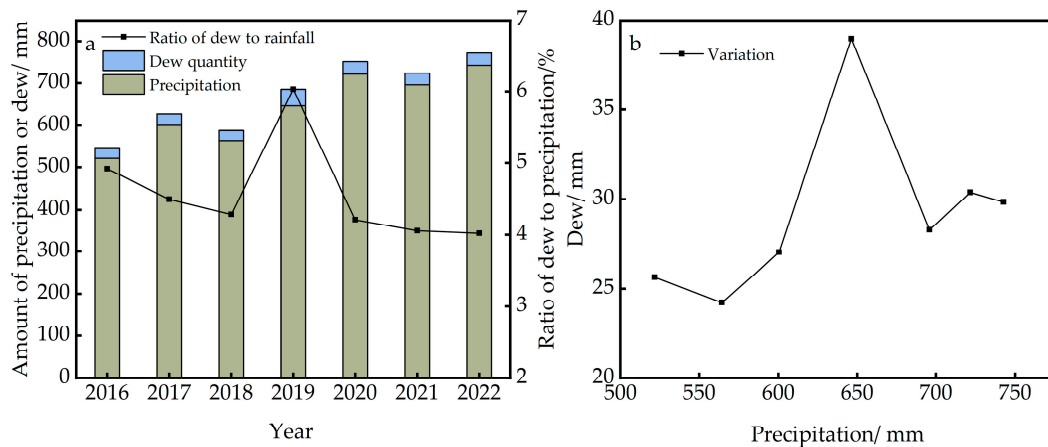


Figure 5. Dew and rainfall trends: (a) interannual variability of dew/rain ratio and (b) trend of dew with precipitation.

According to the dew change from 2016 to 2022 in Table 2, the mean annual dew was 29.20 mm, the mean annual number of dew days was 143.6 d, the mean annual dew frequency was 39.3%, and the mean annual frequency of light dew (58.12%) was greater than that of heavy dew (41.88%). The annual total dew was highest in 2019, followed by 2020, and lowest in 2018. This is because the number of heavy dew days was greater than that of light dew, with the greatest frequency of heavy dew (51.7%) in 2019. Meanwhile, the number of heavy dew days was less than that of light dew in all other years.

Table 2. Interannual dew variation.

Year	Dew Amount/mm	Precipitation/mm	Dew Days/d	Dew Frequency/%	Light Dew 0–0.2 mm		Heavy Dew >0.2 mm	
					Days	Frequency/%	Days	Frequency/%
2016	25.66	521.6	145	39.62	84	57.93	61	42.07
2017	27.02	600.4	132	36.16	69	52.27	63	47.73
2018	24.23	564.2	148	40.55	101	68.24	47	31.76
2019	38.97	646.2	147	40.27	71	48.30	76	51.70
2020	30.38	721.6	152	41.53	89	58.55	63	41.45
2021	28.28	695.8	149	40.82	101	67.79	48	32.21
2022	29.84	742.6	132	36.16	71	53.79	61	46.21
Mean ± SD	29.20 ± 4.83	641.8 ± 77.1	143.6 ± 8.2	39.30 ± 2.22	83.7 ± 13.9	58.12 ± 7.59	60 ± 9.9	41.88 ± 7.59

3.2. Influencing Factors of Dew

3.2.1. Difference between Air Temperature and Dew point

Exponential function fitting was used to obtain the change trend. As shown in Figure 6, the dew tended to increase with a decrease in the temperature dew point difference. When $T_{a20} - T_d \leq 5$ °C, the number of dew days accounted for 88.65% of the total dew days, and the daily amount of dew peaked in this interval. When $T_{a20} - T_d > 8$ °C, less dew occurred. This indicates that dew primarily occurred in the interval where the difference between air temperature and dew point was less than 5 °C.

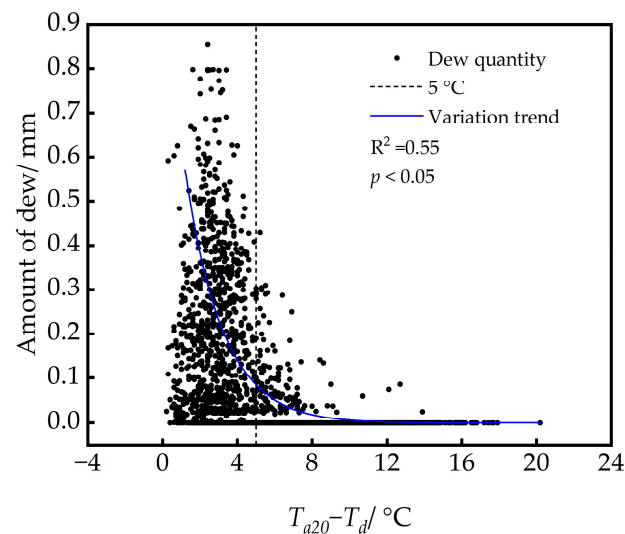


Figure 6. Influence of the air temperature dew point difference on dew.

3.2.2. Relative Humidity

Boltzmann fitting was used to represent the variation characteristics of dew with relative humidity [62]. The Boltzmann equation is often used for the nonlinear fitting of two-dimensional data to represent the variation characteristics of data, and its practicability has been verified [63]. As shown in Figure 7, the amount of dew increased with an increase in the *RH*. When the *RH* was less than 65%, the number of dew days was 40, accounting for 3.98% of the total dew days. When the *RH* was greater than 65%, an increasing trend in the dew amount was evident. When the *RH* was greater than 85%, the daily dew amount peaked. Therefore, an *RH* of 65%–100% more likely resulted in dew formation in the loess hilly region.

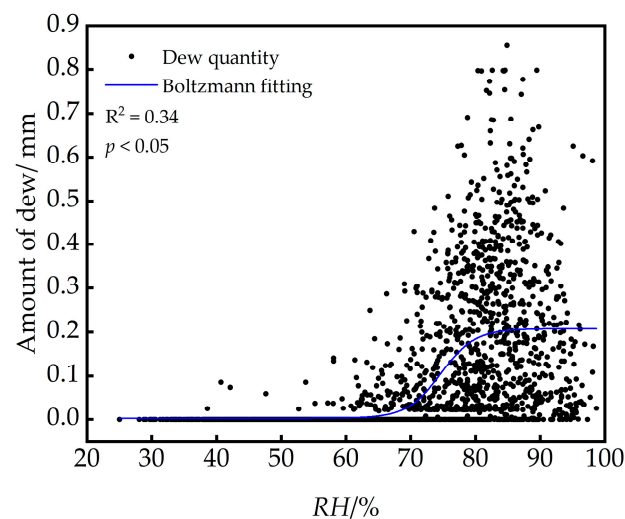


Figure 7. Influence of relative humidity on dew.

3.2.3. Wind Speed and Direction

As shown in Figure 8a,b, the main wind speed range of dew occurrence was $0.01\text{--}1.1\text{ m}\cdot\text{s}^{-1}$, with a percentage of dew days of approximately 85%. The number of dew days and dew frequency differed for different wind speed intervals (Figure 8b). When the wind speed was $0\text{ m}\cdot\text{s}^{-1}$, the number of dew days was 108, accounting for 10.75% of the total. When the wind speed range was $0.01\text{--}0.59\text{ m}\cdot\text{s}^{-1}$, the number of dew days accounted for 63.58% of the total, with the largest dew frequency and the maximum daily

dew amount. When the wind speed was less than $1.1 \text{ m}\cdot\text{s}^{-1}$, the dew frequency was 95.33% of the total. Therefore, the critical wind speed was $1.1 \text{ m}\cdot\text{s}^{-1}$.

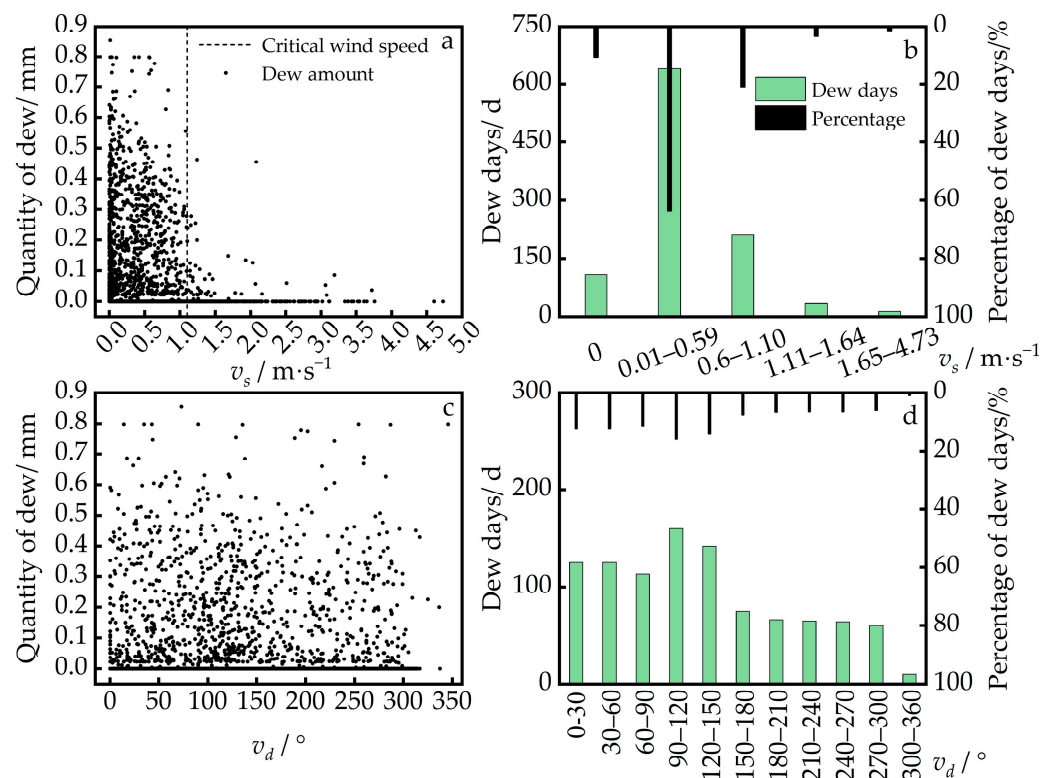


Figure 8. Effects of wind speed and direction on dew: (a) effects of wind speed on dew; (b) distribution of dew within the interval of different wind speeds; (c) effects of wind direction on dew; and (d) distribution of dew within the interval of different wind directions. Percentage of dew days denotes the percentage of dew days out of the total dew days with different wind speeds or wind direction ranges.

The influence of wind direction on the amount and frequency of dew is shown in Figure 8c,d. The main wind directions of dew were $0\text{--}30^\circ$ (northerly wind), $30\text{--}60^\circ$ (north-east wind), $60\text{--}120^\circ$ (easterly wind), and $120\text{--}150^\circ$ (southeast wind), with dew days accounting for 12.44%, 12.44%, 27.16%, and 14.13% of the total, respectively. The daily dew amount reached a maximum in the wind direction range of $0\text{--}150^\circ$.

3.3. Influence of Dew on Soil Moisture

As shown in Figure 9, the soil moisture at different depths responded differently to changes in dew. The surface soil moisture (SWC_0) had a more sensitive dew response and increased synchronously with the increase in the dew amount, with increases of approximately 1.37% (Figure 9a) and 0.68% (Figure 9b), respectively. When the amount of dew reached its peak, the SWC_0 reached its maximum value and remained unchanged for a certain period. In contrast, the change in the 5 cm depth soil moisture (SWC_5) lagged by approximately 1 h. With the increase in dew, the increments of the SWC_5 were small and increased by approximately 0.12% (Figure 9a) and 0.16% (Figure 9b). Therefore, in this study, the main range of soil moisture affected by dew was 0–5 cm. Overall, when the amount of daily dew peaked, the average increased values of SWC_0 and SWC_5 were approximately 1.02% and 0.14%, respectively.

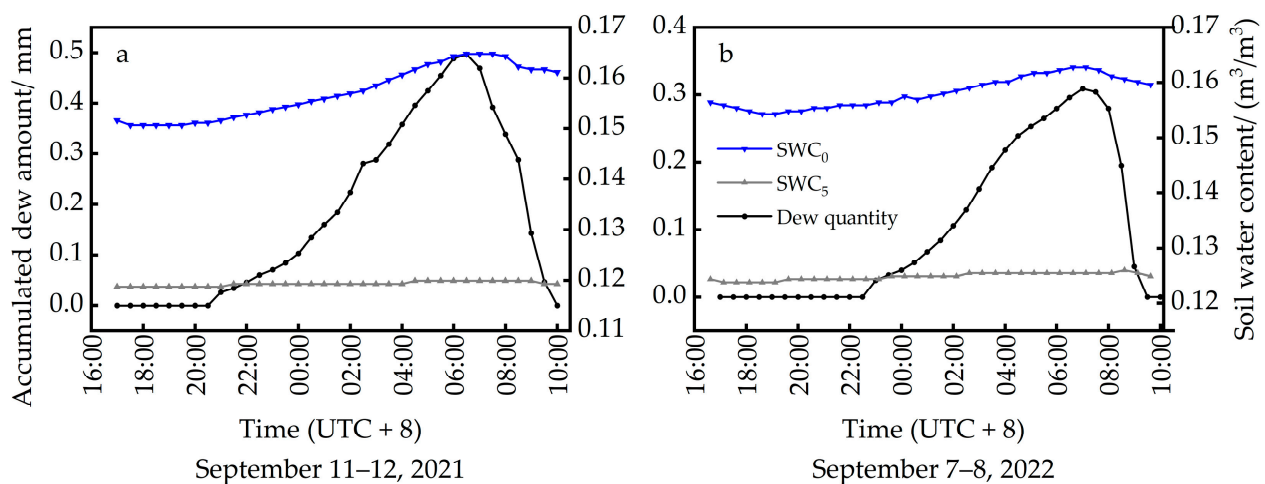


Figure 9. Influence of dew on soil moisture on (a) 11 September 2021, and (b) 7 September 2022. (SWC₀, surface soil moisture; SWC₅, soil moisture 5 cm below the ground surface).

3.4. Simulation and Model Evaluation of Dew

Based on the results of the daily variation analysis of dew, the meteorological data from the main dew occurrence period were selected from 19:00 to 8:00. The Beysens model was used to estimate the dew amount in the study area in 2022. As shown in Table 3, the simulated amount of dew in 2022 was 25.27 mm, and the measured value was 29.84 mm, with an NRMSD of 0.17, indicating a strong simulation effect. The simulation results for the different seasons showed that the Beysens model overestimated the amount of dew in winter, underestimated it in autumn and summer, and satisfactorily simulated it in spring (Table 3). The NRMSD of the simulated and measured dew values for each month were relatively low, except in winter. As shown in Figure 10, the overall simulated monthly dew values ($R^2 = 0.86$, $p < 0.05$) and number of monthly dew days ($R^2 = 0.90$, $p < 0.05$) fit the measured values well. This indicates that the Beysens model can evaluate the amount of dew at both the monthly and annual scales in the study area.

Table 3. Evaluation of Beysens model.

Year–Month	Simulated E_{mi}/mm	Measured D_{mi}/mm	NRMSD	Simulated Dew Days/d	Measured Dew Days/d
2022–1	0.37	0.05	1.49	5	3
2022–2	0.36	0.08	1.22	3	3
2022–3	0.84	0.88	0.19	4	5
2022–4	0.91	1.46	0.20	6	5
2022–5	1.22	1.68	0.21	8	8
2022–6	1.16	1.49	0.26	11	11
2022–7	3.78	6.14	0.33	20	16
2022–8	3.75	4.64	0.35	20	18
2022–9	5.01	7.62	0.20	22	24
2022–10	4.14	3.42	0.24	20	21
2022–11	2.94	2.36	0.36	17	17
2022–12	0.79	0.02	3.07	8	1
Total	25.27	29.84	0.17*	144	132

Note: 0.17* is the annual scale-normalized root-mean-square deviation (NRMSD), calculated based on the simulated and measured values of dew for all remaining days, excluding rainy days in 2022. E_{mi} and D_{mi} denote the simulated and measured dew values for month i , respectively.

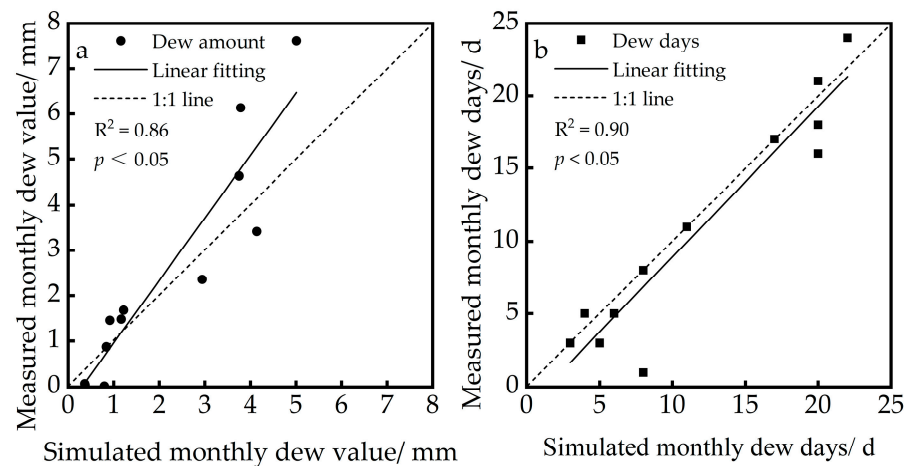


Figure 10. Monthly values simulated by the Beysens model and measured values: (a) dew amount and (b) dew days.

4. Discussion

4.1. Characteristics of Dew in Loess Hilly Areas

The annual mean dew value in the loess hilly areas was 29.20 mm between 2016 and 2022. The main dew occurrence periods were summer and autumn, and the amount and frequency of dew peaked during autumn. The daily variation of dew in different seasons also showed clear seasonal differences. The amount of dew and the duration of dew persistence were the largest in autumn, followed by summer, and smaller in winter and spring. This is consistent with the results of other studies [10,64]. Meanwhile, the daily variation showed that dew primarily occurred from 19:00 to 8:00, with a peak occurring at 5:00–8:00 am and completely disappearing during 8:00–10:00 am. The daily dew variation trend was consistent with that of a field observation experiment conducted at the Yanchi Research Station, Ningxia, in the Mu Us Desert, China [65].

4.2. Factors Affecting Dew in Loess Hilly Areas

The formation of dew is closely related to thermodynamics and aerodynamics, primarily influenced by micrometeorological factors, such as air temperature, RH , and wind speed in near-surface ecosystems [66–68]. RH is a necessary condition for the occurrence of dew, and different regions have different RH thresholds. In a typical gravelly desert ecosystem in Linze, China, the RH threshold for dew was 30% [39]. A dew observation experiment in Dingxi, Gansu, China, found that dew occurred when the RH was greater than 60% [36]. By analyzing field observation data from 2016–2022, this study found that the threshold for dew occurrence in the study area was RH greater than 65%. When the RH was less than 65%, the number of dew days accounted for only 3.98% of the total, with a low frequency of occurrence and no prominent increasing trend in the dew amount.

Meanwhile, an air temperature dew point difference lower than $5\text{ }^{\circ}\text{C}$ was the main occurrence interval range for dew, the days of which comprised 88.65% of the total dew days. Similarly, water vapor condensation occurred when the temperature dew point difference was approximately $3\text{ }^{\circ}\text{C}$, which are not ideal conditions for a temperature below the dew point [26,69,70]. In a dew observation experiment at the Shapotou Desert Experimental Research Station in China, dew still occurred at a temperature dew point difference of $12\text{ }^{\circ}\text{C}$ [71].

In this study, the wind speed range of $0.01\text{--}1.1\text{ m}\cdot\text{s}^{-1}$ at 200 cm was favorable for the occurrence of dew in the loess hilly area. This is close to the wind speed range of $0.15\text{--}2.0\text{ m}\cdot\text{s}^{-1}$ reported by Zhuang et al. [39]. When the wind speed was greater than $3.75\text{ m}\cdot\text{s}^{-1}$, there was no dew occurrence. This is consistent with past studies that showed that it was difficult for condensation to occur when the surface wind speed was beyond $4.5\text{ m}\cdot\text{s}^{-1}$ [65,72]. Moderate wind speeds can promote water vapor transport and ensure

that the condensation surface maintains a low temperature, which helps dew to occur [36]. Wind speeds that are too high could reduce water vapor around the condensation surface, which is not conducive to dew formation [73].

4.3. Applicability of the Beysens Model

The estimation results using the Beysens model for the different regions differed. In this study, the amount of dew estimated using the Beysens model was 15.3% lower than the measured value. In a study of the Hunsandak Sandy Land, Inner Mongolia, China, the values simulated using the Beysens model were approximately 6.2% higher than the measured values [74]. In the Mediterranean Basin dew test, the values estimated by the Beysens model were approximately 7.0% lower than the measured values [24]. The Beysens model primarily uses meteorological factors, that is, wind speed, cloudiness, *RH*, and air temperature. Natural convection and forced (wind) convection cause heat exchange between the condensation surface and the air variable, such that larger dew events tend to be underestimated, whereas smaller dew events tend to be overestimated [24,52].

4.4. Impacts of Dew on Ecosystems

The ratio of annual dew to annual rainfall varies with different regional and climatic conditions in arid regions with scarce rainfall and low vegetation cover. According to a study in the Negev Desert of Israel, the local annual dew-to-rain ratio could be as high as 36% [37]. Meanwhile, the amount of dew in the Hunshandak Sandy Land in Duolun County, Inner Mongolia, China, was approximately 5% of the annual rainfall [74]. A study in Tengger Desert in Shapotou, China showed that the condensation amounted to 11.46%–17.67% of the rainfall [75]. In this study, the average annual dew-to-rain ratio in the loess hilly area was 4.58% from 2016 to 2022. Unlike rainfall, dew is a continuous and stable water source, although it provides smaller amounts [76]. In addition to precipitation, dew is an important source of water that plays a key role in maintaining the regional water balance [77,78]. Dew from plant leaves can be absorbed by plants, improving their internal water status and reducing the water deficit caused by plant evaporation [79–81]. Dew can significantly increase aboveground plant biomass and store sufficient nutrients for flowering and fruiting [82]. A study in the loess hilly areas of China found that dew, as a vital water resource, was crucial for jujube trees [83]. In this study, dew increased the SWC within 0–5 cm of the soil surface, which can regulate and improve the surface water balance. This improves the local microclimate and promotes the growth and development of surface vegetation [84,85]. Dew has important effects on the physiological activities of meiofauna and microorganisms in arid regions [9,12,86,87]. In the Namib Desert region of Africa, tenebrionid beetles (*Stenocara* sp.) can replenish bodily water by increasing the amount of dew through uneven sheath wings on their dorsum [88]. Experiments in semi-arid grasslands in Arizona, USA, and the Mediterranean region have shown that dew can effectively stimulate microbial activity and promote litter decomposition and carbon cycling processes [86,89]. Therefore, as a non-precipitation water resource, dew has a significant impact on plant and animal survival [90,91] and crop production [19,83] in arid regions.

5. Conclusions

This study conducted long-term field observation experiments from 2016 to 2022 at the Ansai Experimental Station in a typical loess hilly area of China to explore the characteristics of dew and used the Beysens model to evaluate the dew amount. The main conclusions are as follows.

(1) The average annual dew days and dew amounts were 143.6 d and 29.20 mm, respectively, with an average annual dew-to-rain ratio of 4.58%. Dew primarily occurred in summer and autumn, with less in winter and spring.

(2) The occurrence of dew was more likely with a difference between the air temperature and dew point of less than 5 °C, RH of more than 65%, and wind speed of less than 1.1 m·s⁻¹.

(3) Dew had different effects on the SWC at different depths. When the daily dew amount peaked, it could increase the SWC₀ by approximately 1.02%, and the SWC₅ by approximately 0.14%.

(4) The Beysens model can accurately evaluate the dew quantity in the study area at both the monthly and annual scales.

Author Contributions: Conceptualization, Z.J. and Z.G.; methodology, Y.C., H.L., G.L. and X.Z.; software, Y.C., R.X. and H.L.; validation, Z.J., Z.G., P.L. and Y.L.; investigation, Y.C., P.L., G.L. and X.Z.; writing—original draft preparation, Z.J. and Y.C.; writing—review and editing, Z.J., Y.C. and Z.G. All authors have read and agreed to the published version of the manuscript.

Funding: This work was supported by the National Natural Science Foundation of China (42001033), the Natural Science Basic Research Plan in the Shaanxi Province of China (2021JQ-237), and the Fundamental Research Funds for the Central Universities, CHD (300102293209).

Institutional Review Board Statement: Not applicable.

Informed Consent Statement: Not applicable.

Data Availability Statement: Data are contained within the article.

Conflicts of Interest: Authors Zilong Guan and Xingchen Zhang were employed by the company PowerChina Northwest Engineering Corp Ltd.; Author Pengcheng Liu was employed by the Xi'an Water (Group) Lijiahe Reservoir Management Company. The remaining authors declare that the research was conducted in the absence of any commercial or financial relationships that could be construed as a potential conflict of interest.

References

1. Cao, S.; Chen, L.; Yu, X. Impact of China's Grain for Green Project on the landscape of vulnerable arid and semi-arid agricultural regions: A case study in northern Shaanxi Province. *J. Appl. Ecol.* **2009**, *46*, 536–543. [\[CrossRef\]](#)
2. Zhao, Y.; Xu, M. Runoff and Soil Loss from Revegetated Grasslands in the Hilly Loess Plateau Region, China: Influence of Biocrust Patches and Plant Canopies. *J. Hydrol. Eng.* **2013**, *18*, 387–393. [\[CrossRef\]](#)
3. Gao, L.; Bowker, M.A.; Xu, M.; Sun, H.; Tuo, D.; Zhao, Y. Biological soil crusts decrease erodibility by modifying inherent soil properties on the Loess Plateau, China. *Soil Biol. Biochem.* **2017**, *105*, 49–58. [\[CrossRef\]](#)
4. Xiao, B.; Ma, S.; Hu, K. Moss biocrusts regulate surface soil thermal properties and generate buffering effects on soil temperature dynamics in dryland ecosystem. *Geoderma* **2019**, *351*, 9–24. [\[CrossRef\]](#)
5. Tsafaras, I.; Campen, J.B.; de Zwart, H.F.; Voogt, W.; Harbi, A.A.; Assaf, K.A.; Abdelaziz, M.E.; Qaryouti, M.; Stanghellini, C. Quantifying the trade-off between water and electricity for tomato production in arid environments. *Agric. Water Manag.* **2022**, *271*, 107819. [\[CrossRef\]](#)
6. Kidron, G.J. Analysis of dew precipitation in three habitats within a small arid drainage basin, Negev Highlands, Israel. *Atmos. Res.* **2000**, *55*, 257–270. [\[CrossRef\]](#)
7. Fang, X.; Zhao, W.; Wang, L.; Feng, Q.; Ding, J.; Liu, Y.; Zhang, X. Variations of deep soil moisture under different vegetation types and influencing factors in a watershed of the Loess Plateau, China. *Hydrol. Earth Syst. Sci.* **2016**, *20*, 3309–3323. [\[CrossRef\]](#)
8. Hill, A.J.; Dawson, T.E.; Shelef, O.; Rachmilevitch, S. The role of dew in Negev Desert plants. *Oecologia* **2015**, *178*, 317–327. [\[CrossRef\]](#)
9. Jacobs, A.F.G.; Heusinkveld, B.G.; Berkowicz, S. Dew deposition and drying in a desert system: A simple simulation model. *J. Arid. Environ.* **1999**, *42*, 211–222. [\[CrossRef\]](#)
10. Hao, X.-M.; Li, C.; Guo, B.; Ma, J.-X.; Ayup, M.; Chen, Z.-S. Dew formation and its long-term trend in a desert riparian forest ecosystem on the eastern edge of the Taklimakan Desert in China. *J. Hydrol.* **2012**, *472–473*, 90–98. [\[CrossRef\]](#)
11. Agam, N.; Berliner, P.R. Dew formation and water vapor adsorption in semi-arid environments—A review. *J. Arid Environ.* **2006**, *65*, 572–590. [\[CrossRef\]](#)
12. Wang, L.; Kaseke, K.F.; Seely, M.K. Effects of non-rainfall water inputs on ecosystem functions. *Wiley Interdiscip. Rev. Water* **2017**, *4*, e1179. [\[CrossRef\]](#)
13. Feng, T.; Zhang, L.; Chen, Q.; Ma, Z.; Wang, H.; Shangguan, Z.; Wang, L.; He, J.-S. Dew formation reduction in global warming experiments and the potential consequences. *J. Hydrol.* **2021**, *593*, 12589. [\[CrossRef\]](#)
14. Kidron, G.J.; Starinsky, A. Measurements and ecological implications of non-rainfall water in desert ecosystems—A review. *Ecohydrology* **2019**, *12*, e2121. [\[CrossRef\]](#)

15. Ninari, N.; Berliner, P.R. The role of dew in the water and heat balance of bare loess soil in the Negev Desert: Quantifying the actual dew deposition on the soil surface. *Atmos. Res.* **2002**, *64*, 323–334. [[CrossRef](#)]
16. Guo, X.; Wang, Y.; Yan, H.; Liu, P.; Tian, Y.; Shang, G.; Jin, C.; Zha, T. Dew/hoar frost on the canopies and underlying surfaces of two typical desert shrubs in Northwest China and their relevance to drought. *J. Hydrol.* **2022**, *609*, 127880. [[CrossRef](#)]
17. Jia, Z.; Wang, Z.; Wang, H. Characteristics of Dew Formation in the Semi-Arid Loess Plateau of Central Shaanxi Province, China. *Water* **2019**, *11*, 126. [[CrossRef](#)]
18. Cosh, M.H.; Kabela, E.D.; Hornbuckle, B.; Gleason, M.L.; Jackson, T.J.; Prueger, J.H. Observations of dew amount using in situ and satellite measurements in an agricultural landscape. *Agric. For. Meteorol.* **2009**, *149*, 1082–1086. [[CrossRef](#)]
19. Gao, Z.; Shi, W.; Wang, X.; Wang, Y. Non-rainfall water contributions to dryland jujube plantation evapotranspiration in the Hilly Loess Region of China. *J. Hydrol.* **2020**, *583*, 124604. [[CrossRef](#)]
20. Khabbazan, S.; Steele-Dunne, S.C.; Vermunt, P.; Judge, J.; Vreugdenhil, M.; Gao, G. The influence of surface canopy water on the relationship between L-band backscatter and biophysical variables in agricultural monitoring. *Remote Sens. Environ.* **2022**, *268*, 112789. [[CrossRef](#)]
21. Binks, O.; Mencuccini, M.; Rowland, L.; da Costa, A.C.L.; de Carvalho, C.J.R.; Bittencourt, P.; Eller, C.; Teodoro, G.S.; Carvalho, E.J.M.; Soza, A.; et al. Foliar water uptake in Amazonian trees: Evidence and consequences. *Global Chang. Biol.* **2019**, *25*, 2678–2690. [[CrossRef](#)]
22. Allen, R.G.; Pereira, L.S.; Raes, D.; Smith, M. *Crop Evapotranspiration: Guidelines for Computing Crop Water Requirements*; FAO: Rome, Italy, 1998.
23. Papale, D.; Reichstein, M.; Aubinet, M.; Canfora, E.; Bernhofer, C.; Kutsch, W.L.; Longdoz, B.; Rambal, S.; Valentini, R.; Vesala, T.; et al. Towards a standardized processing of Net Ecosystem Exchange measured with eddy covariance technique: Algorithms and uncertainty estimation. *Biogeosciences* **2006**, *3*, 571–583. [[CrossRef](#)]
24. Tomaszewicz, M.; Abou Najm, M.; Beysens, D.; Alameddine, I.; Bou Zeid, E.; El-Fadel, M. Projected climate change impacts upon dew yield in the Mediterranean basin. *Sci. Total Environ.* **2016**, *566–567*, 1339–1348. [[CrossRef](#)] [[PubMed](#)]
25. Lekouch, I.; Lekouch, K.; Muselli, M.; Mongruel, A.; Kabbachi, B.; Beysens, D. Rooftop dew, fog and rain collection in southwest Morocco and predictive dew modeling using neural networks. *J. Hydrol.* **2012**, *448–449*, 60–72. [[CrossRef](#)]
26. Beysens, D. Estimating dew yield worldwide from a few meteo data. *Atmos. Res.* **2016**, *167*, 146–155. [[CrossRef](#)]
27. Zheng, Y.; Bai, H.; Huang, Z.; Tian, X.; Nie, F.-Q.; Zhao, Y.; Zhai, J.; Jiang, L. Directional water collection on wetted spider silk. *Nature* **2010**, *463*, 640–643. [[CrossRef](#)] [[PubMed](#)]
28. Pan, Z.; Pitt, W.G.; Zhang, Y.; Wu, N.; Tao, Y.; Truscott, T.T. The upside-down water collection system of *Syntrichia caninervis*. *Nat. Plants* **2016**, *2*, 16076. [[CrossRef](#)] [[PubMed](#)]
29. Tuure, J.; Korpela, A.; Hautala, M.; Rautkoski, H.; Hakojärvi, M.; Mikkola, H.; Duplissy, J.; Pellikka, P.; Petäjä, T.; Kulmala, M.; et al. Comparing plastic foils for dew collection: Preparatory laboratory-scale method and field experiment in Kenya. *Biosyst. Eng.* **2020**, *196*, 145–158. [[CrossRef](#)]
30. Kool, D.; Agra, E.; Drabkin, A.; Duncan, A.; Fendinat, P.P.; Leduc, S.; Lupovitch, G.; Nambwandja, A.N.; Ndilenga, N.S.; Nguyễn Thị, T.; et al. The overlooked non-rainfall water input sibling of fog and dew: Daily water vapor adsorption on a !Nara hummock in the Namib Sand Sea. *J. Hydrol.* **2021**, *598*, 126420. [[CrossRef](#)]
31. Riedl, A.; Li, Y.; Eugster, J.; Buchmann, N.; Eugster, W. Technical note: High-accuracy weighing micro-lysimeter system for long-term measurements of non-rainfall water inputs to grasslands. *Hydrol. Earth Syst. Sci.* **2022**, *26*, 91–116. [[CrossRef](#)]
32. Gerlein-Safdi, C.; Koohafkan, M.C.; Chung, M.; Rockwell, F.E.; Thompson, S.; Caylor, K.K. Dew deposition suppresses transpiration and carbon uptake in leaves. *Agric. For. Meteorol.* **2018**, *259*, 305–316. [[CrossRef](#)]
33. Juříčka, D.; Pecina, V.; Kusbach, A.; Vlček, V.; Novotná, J.; Pařílková, J.; Otgonsuren, B.; Brtnický, M.; Kynický, J. Thermal regime of semi-natural dew collector’s perspective for afforestation of semi-arid landscapes. *Environ. Technol. Innov.* **2020**, *20*, 101125. [[CrossRef](#)]
34. Maestre-Valero, J.F.; Martín-Gorriz, B.; Martínez-Alvarez, V. Dew condensation on different natural and artificial passive surfaces in a semi-arid climate. *J. Arid Environ.* **2015**, *116*, 63–70. [[CrossRef](#)]
35. Jacobs, A.F.G.; Heusinkveld, B.G.; Wichink Kruit, R.J.; Berkowicz, S.M. Contribution of dew to the water budget of a grassland area in the Netherlands. *Water Resour. Res.* **2006**, *42*, W03415. [[CrossRef](#)]
36. Zhang, Q.; Wang, S.; Yang, F.-L.; Yue, P.; Yao, T.; Wang, W.-Y. Characteristics of Dew Formation and Distribution, and Its Contribution to the Surface Water Budget in a Semi-Arid Region in China. *Boundary-Layer Meteorol.* **2015**, *154*, 317–331. [[CrossRef](#)]
37. Kidron, G.J. Altitude dependent dew and fog in the Negev Desert, Israel. *Agric. For. Meteorol.* **1999**, *96*, 1–8. [[CrossRef](#)]
38. Gotsch, S.G.; Asbjornsen, H.; Holwerda, F.; Goldsmith, G.R.; Weintraub, A.E.; Dawson, T.E. Foggy days and dry nights determine crown-level water balance in a seasonal tropical Montane cloud forest. *Plant Cell Environ.* **2014**, *37*, 261–272. [[CrossRef](#)]
39. Zhuang, Y.; Zhao, W.; Luo, L.; Wang, L. Dew formation characteristics in the gravel desert ecosystem and its ecological roles on *Reaumuria soongorica*. *J. Hydrol.* **2021**, *603*, 126932. [[CrossRef](#)]
40. Jia, Z.; Lei, R.; Liu, Y.; Liu, P.; Wang, Z.; Chang, Y.; Wei, W. Spatial–Temporal Variations and the Driving Factors of Vegetation Coverage in the Loess Hilly and Gully Region of China. *Forests* **2023**, *14*, 1238. [[CrossRef](#)]
41. Zhao, D.; Xu, M.; Liu, G.; Yao, X.; Tuo, D.; Zhang, R.; Xiao, T.; Peng, G. Quantification of soil aggregate microstructure on abandoned cropland during vegetative succession using synchrotron radiation-based micro-computed tomography. *Soil Tillage Res.* **2017**, *165*, 239–246. [[CrossRef](#)]

42. Hua, L.; Gao, J.; Zhou, M.; Bai, S. Impacts of Relative Elevation on Soil Nutrients and Apple Quality in the Hilly-Gully Region of the Loess Plateau, China. *Sustainability* **2021**, *13*, 1293. [CrossRef]
43. Feng, Q.; Dong, S.; Duan, B. The Effects of Land-Use Change/Conversion on Trade-Offs of Ecosystem Services in Three Precipitation Zones. *Sustainability* **2021**, *13*, 13306. [CrossRef]
44. *VP-3 Operators Manual*; Decagon Devices, Inc.: Pullman, WA, USA, 2015; Volume 8–9.
45. Li, Q.; Liu, J.; Wang, S.; Guo, Y.; Han, X.; Li, Q.; Cheng, Y.; Dong, Z.; Li, X.; Zhang, X. Numerical insights into factors affecting collapse behavior of horizontal wellbore in clayey silt hydrate-bearing sediments and the accompanying control strategy. *Ocean Eng.* **2024**, *297*, 117029. [CrossRef]
46. Li, Q.; Wang, F.; Wang, Y.; Forson, K.; Cao, L.; Zhang, C.; Zhou, C.; Zhao, B.; Chen, J. Experimental investigation on the high-pressure sand suspension and adsorption capacity of guar gum fracturing fluid in low-permeability shale reservoirs: Factor analysis and mechanism disclosure. *Environ. Sci. Pollut. Res.* **2022**, *29*, 53050–53062. [CrossRef] [PubMed]
47. Lawrence, M.G. The Relationship between Relative Humidity and the Dewpoint Temperature in Moist Air: A Simple Conversion and Applications. *Bull. Am. Meteorol. Soc.* **2005**, *86*, 225–234. [CrossRef]
48. Alduchov, O.A.; Eskridge, R.E. Improved Magnus form approximation of saturation vapor pressure. *J. Appl. Meteorol.* **1996**, *35*, 601–609. [CrossRef]
49. Copernicus Climate Data Store. Available online: <https://cds.climate.copernicus.eu> (accessed on 10 January 2024).
50. WMO. *Manual on Codes. Part A—Alphanumeric Codes*; Secretariat of the World Meteorological Organization: Geneva, Switzerland, 1995.
51. Kotarba, A.Z. Inconsistency of surface-based (SYNOP) and satellite-based (MODIS) cloud amount estimations due to the interpretation of cloud detection results. *Int. J. Clim.* **2017**, *37*, 4092–4104. [CrossRef]
52. Muselli, M.; Lekouch, I.; Beysens, D. Physical and Chemical Characteristics of Dew and Rain in North-West Africa with Focus on Morocco: Mapping Past and Future Evolution (2005–2100). *Atmosphere* **2022**, *13*, 1974. [CrossRef]
53. Berger, X.; Bathiebo, J.; Kieno, F.; Awanou, C.N. Clear sky radiation as a function of altitude. *Renew. Energ.* **1992**, *2*, 139–157. [CrossRef]
54. Top, C.B. A Generalized Split-Step Angular Spectrum Method for Efficient Simulation of Wave Propagation in Heterogeneous Media. *IEEE Trans. Ultrason. Ferroelectr. Freq. Control.* **2021**, *68*, 2687–2696. [CrossRef] [PubMed]
55. Franceschelli, L.; Ciricugno, C.; Di Lorenzo, M.; Romani, A.; Berardinelli, A.; Tartagni, M.; Correale, R. Real-time gas mass spectroscopy by multivariate analysis. *Sci. Rep.* **2023**, *13*, 6059. [CrossRef]
56. Kang, Y.-S.; Goldman, S.; Moorhouse, K.; Bolte, J. Evaluation of a coplanar 6a3 ω configuration in the Hybrid III 50th percentile male head. *Traffic Inj. Prev.* **2017**, *18*, S129–S135. [CrossRef] [PubMed]
57. Fang, X.; Pomeroy, J.W. Impact of antecedent conditions on simulations of a flood in a mountain headwater basin. *Hydrol. Process.* **2016**, *30*, 2754–2772. [CrossRef]
58. Mobini, N.; Malekzadeh, M.; Haghghatkah, H.; Saligheh Rad, H. A hybrid (iron–fat–water) phantom for liver iron overload quantification in the presence of contaminating fat using magnetic resonance imaging. *Magn. Reson. Mater. Phys.* **2019**, *33*, 385–392. [CrossRef] [PubMed]
59. Burgund, D.; Nikolovski, S.; Galić, D.; Maravić, N. Pearson Correlation in Determination of Quality of Current Transformers. *Sensors* **2023**, *23*, 2704. [CrossRef] [PubMed]
60. Liu, Y.; Wu, J.; Huang, T.; Nie, W.; Jia, Z.; Gu, Y.; Ma, X. Study on the relationship between regional soil desertification and salinization and groundwater based on remote sensing inversion: A case study of the windy beach area in Northern Shaanxi. *Sci. Total Environ.* **2024**, *912*, 168854. [CrossRef]
61. Salau, O.A.; Lawson, T.L. Dewfall features of a tropical station: The case of Onne (Port Hartcourt), Nigeria. *Theor. Appl. Climatol.* **1986**, *37*, 233–240. [CrossRef]
62. Fang, J. Variability in condensation water and its determinants in arid regions of north-western China. *Ecolhydrology* **2020**, *13*, e2226. [CrossRef]
63. Heusser, K.; Heusser, R.; Jordan, J.; Urech, V.; Diedrich, A.; Tank, J. Baroreflex Curve Fitting Using a WYSIWYG Boltzmann Sigmoidal Equation. *Front. Neurosci.* **2021**, *15*, 697582. [CrossRef]
64. Scherm, H.; Bruggen, A.H.C.v. Sensitivity of simulated dew duration to meteorological variations in different climatic regions of California. *Agric. For. Meteorol.* **1993**, *66*, 229–245. [CrossRef]
65. Guo, X.; Zha, T.; Jia, X.; Wu, B.; Feng, W.; Xie, J.; Gong, J.; Zhang, Y.; Peltola, H. Dynamics of Dew in a Cold Desert-Shrub Ecosystem and Its Abiotic Controls. *Atmosphere* **2016**, *7*, 32. [CrossRef]
66. Zangvil, A. Six years of dew observations in the Negev Desert, Israel. *J. Arid Environ.* **1996**, *32*, 361–371. [CrossRef]
67. Kaseke, K.F.; Wang, L.X.; Seely, M.K. Nonrainfall water origins and formation mechanisms. *Sci. Adv.* **2017**, *3*, e1603131. [CrossRef] [PubMed]
68. Sharan, G.; Beysens, D.; Milimouk-Melnytchouk, I. A study of dew water yields on Galvanized iron roofs in Kothara (North-West India). *J. Arid Environ.* **2007**, *69*, 259–269. [CrossRef]
69. Li, S.L.; Bowker, M.A.; Xiao, B. Biocrusts enhance non-rainfall water deposition and alter its distribution in dryland soils. *J. Hydrol.* **2021**, *595*, 126050. [CrossRef]
70. Agam, N.; Berliner, P. Diurnal Water Content Changes in the Bare Soil of a Coastal Desert. *J. Hydrometeorol.* **2004**, *5*, 922–933. [CrossRef]

71. Wang, X.P.; Pan, Y.X.; Hu, R.; Zhang, Y.F.; Zhang, H. Condensation of water vapour on moss-dominated biological soil crust, NW China. *J. Earth Syst. Sci.* **2014**, *123*, 297–305. [[CrossRef](#)]
72. Muselli, M.; Beysens, D.; Marcillat, J.; Milimouk, I.; Nilsson, T.; Louche, A. Dew water collector for potable water in Ajaccio (Corsica Island, France). *Atmos. Res.* **2002**, *64*, 297–312. [[CrossRef](#)]
73. Vuollekoski, H.; Vogt, M.; Sinclair, V.A.; Duplissy, J.; Järvinen, H.; Kyrö, E.M.; Makkonen, R.; Petäjä, T.; Prisle, N.L.; Räisänen, P.; et al. Estimates of global dew collection potential on artificial surfaces. *Hydrol. Earth Syst. Sci.* **2015**, *19*, 601–613. [[CrossRef](#)]
74. Liu, M.; Cen, Y.; Wang, C.; Gu, X.; Bowler, P.; Wu, D.; Zhang, L.; Jiang, G.; Beysens, D. Foliar uptake of dew in the sandy ecosystem of the Mongolia Plateau: A life-sustaining and carbon accumulation strategy shared differently by C3 and C4 grasses. *Agric. For. Meteorol.* **2020**, *287*, 107941. [[CrossRef](#)]
75. Jia, R.L.; Li, X.R.; Liu, L.C.; Pan, Y.X.; Gao, Y.H.; Wei, Y.P. Effects of sand burial on dew deposition on moss soil crust in a revegetated area of the Tennger Desert, Northern China. *J. Hydrol.* **2014**, *519*, 2341–2349. [[CrossRef](#)]
76. Zhuang, Y.; Zhao, W. Dew formation and its variation in *Haloxylon ammodendron* plantations at the edge of a desert oasis, northwestern China. *Agric. For. Meteorol.* **2017**, *247*, 541–550. [[CrossRef](#)]
77. Kidron, G.J.; Kronenfeld, R. Assessing the effect of micro-lysimeters on NRWI: Do micro-lysimeters adequately represent the water input of natural soil? *J. Hydrol.* **2017**, *548*, 382–390. [[CrossRef](#)]
78. Aguirre-Gutiérrez, C.A.; Holwerda, F.; Goldsmith, G.R.; Delgado, J.; Yopez, E.; Carbajal, N.; Escoto-Rodríguez, M.; Arredondo, J.T. The importance of dew in the water balance of a continental semiarid grassland. *J. Arid Environ.* **2019**, *168*, 26–35. [[CrossRef](#)]
79. Munné-Bosch, S.; Alegre, L. Role of Dew on the Recovery of Water-Stressed *Melissa officinalis* L. Plants. *J. Plant Physiol.* **1999**, *154*, 759–766. [[CrossRef](#)]
80. Eller, C.B.; Lima, A.L.; Oliveira, R.S. Foliar uptake of fog water and transport belowground alleviates drought effects in the cloud forest tree species, *Drimys brasiliensis* (Winteraceae). *New Phytol.* **2013**, *199*, 151–162. [[CrossRef](#)] [[PubMed](#)]
81. Dawson, T.E.; Goldsmith, G.R. The value of wet leaves. *New Phytol.* **2018**, *219*, 1156–1169. [[CrossRef](#)]
82. Zhuang, Y.; Ratcliffe, S. Relationship between dew presence and *Bassia dasyphylla* plant growth. *J. Arid Land* **2012**, *4*, 11–18. [[CrossRef](#)]
83. Wang, X.; Gao, Z.Y.; Wang, Y.K.; Wang, Z.; Jin, S.S. Dew measurement and estimation of rain-fed jujube (*Zizyphus jujube* Mill) in a semi-arid loess hilly region of China. *J. Arid Land* **2017**, *9*, 547–557. [[CrossRef](#)]
84. Ye, Y.; Zhou, K.; Song, L.; Jin, J.; Peng, S. Dew amounts and its correlations with meteorological factors in urban landscapes of Guangzhou, China. *Atmos. Res.* **2007**, *86*, 21–29. [[CrossRef](#)]
85. Gutterman, Y.; Shem-Tov, S. Mucilaginous seed coat structure of *Carrichtera annua* and *Anastatica hierochuntica* from the Negev Desert highlands of Israel, and its adhesion to the soil crust. *J. Arid Environ.* **1997**, *35*, 695–705. [[CrossRef](#)]
86. McHugh, T.A.; Morrissey, E.M.; Reed, S.C.; Hungate, B.A.; Schwartz, E. Water from air: An overlooked source of moisture in arid and semiarid regions. *Sci. Rep.* **2015**, *5*, 13767. [[CrossRef](#)] [[PubMed](#)]
87. Rao, B.D.; Liu, Y.; Wang, W.; Hu, C.; Dun-hai, L.; Lan, S. Influence of dew on biomass and photosystem II activity of cyanobacterial crusts in the Hopq Desert, northwest China. *Soil Biol. Biochem.* **2009**, *41*, 2387–2393. [[CrossRef](#)]
88. Parker, A.R.; Lawrence, C.R. Water capture by a desert beetle. *Nature* **2001**, *414*, 33–34. [[CrossRef](#)]
89. Gliksmann, D.; Rey, A.; Seligmann, R.; Dumbur, R.; Sperling, O.; Navon, Y.; Haenel, S.; De Angelis, P.; Arnone, J.A.; Grünzweig, J.M. Biotic degradation at night, abiotic degradation at day: Positive feedbacks on litter decomposition in drylands. *Glob. Chang. Biol.* **2017**, *23*, 1564–1574. [[CrossRef](#)]
90. Kaseke, K.F.; Wang, L. Fog and Dew as Potable Water Resources: Maximizing Harvesting Potential and Water Quality Concerns. *Geohealth* **2018**, *2*, 327–332. [[CrossRef](#)]
91. Ben-Asher, J.; Alpert, P.; Ben-Zvi, A. Dew is a major factor affecting vegetation water use efficiency rather than a source of water in the eastern Mediterranean area. *Water Resour. Res.* **2010**, *46*, W10532. [[CrossRef](#)]

Disclaimer/Publisher’s Note: The statements, opinions and data contained in all publications are solely those of the individual author(s) and contributor(s) and not of MDPI and/or the editor(s). MDPI and/or the editor(s) disclaim responsibility for any injury to people or property resulting from any ideas, methods, instructions or products referred to in the content.